© 2014. Published by The Company of Biologists Ltd | The Journal of Experimental Biology (2014) 217, 1 doi:10.1242/jeb.105585

CORRECTION

# Adjustments of global and local hindlimb properties during the terrestrial locomotion of the common quail (*Coturnix coturnix*)

**Emanuel Andrada, John A. Nyakatura, Florian Bergmann and Reinhard Blickhan**

There was an error published in *J. Exp. Biol.* **216**, pp. 3906-3916.

In Fig. 7, the mean values of the joint torques in the middle and the right column were erroneously displayed as Nm $BW^{-1}$. The units should have been Nm $kg^{-1}$. The correct figure is printed below.

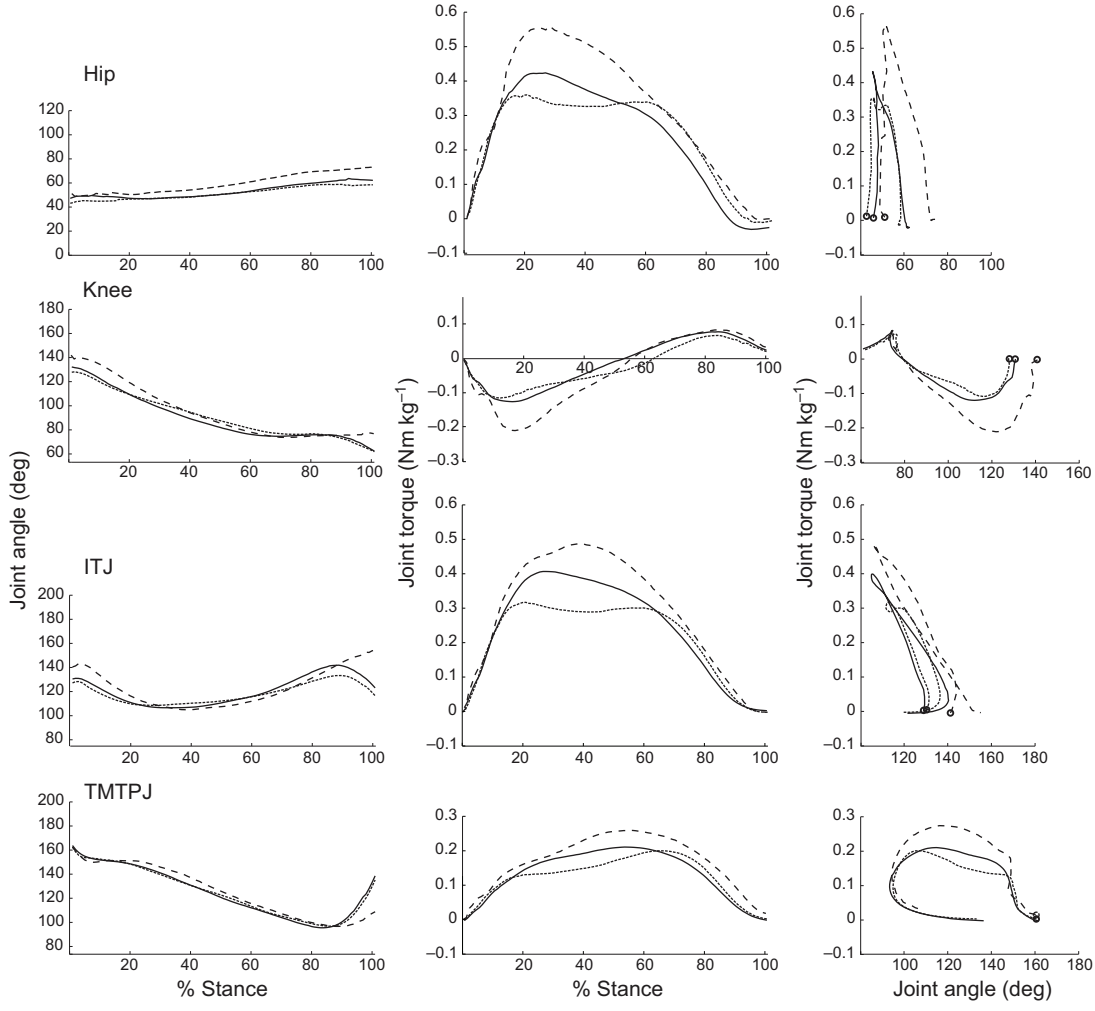


Fig. 7. Local leg parameters (joint mechanics) during terrestrial locomotion of the quail (walking, dotted line; grounded running, solid line; running, dashed line). Joint angles (left), joint torques (middle) and torque–angle plots (right) over the course of the stance for the hip, knee, ITJ and TMTJ. Displayed are mean values (walking, 32 strides; grounded running, 34 strides; running, eight strides). Increasing joint angles indicate extension, and positive values in the torque plots represent extensor torques. Circles indicate touch-down.

We apologise to readers for any inconvenience that this error may have caused.

The Journal of Experimental Biology 216, 3906-3916

doi:10.1242/jeb.085399

## RESEARCH ARTICLE

# Adjustments of global and local hindlimb properties during terrestrial locomotion of the common quail (*Coturnix coturnix*)

Emanuel Andrada[1,*], John A. Nyakatura[2], Florian Bergmann[1] and Reinhard Blickhan[1]

[1]Department of Science of Motion, Friedrich Schiller University Jena, Seidelstraße 20, D-07749 Jena, Germany and
[2]Institute of Systematic Zoology and Evolutionary Biology with Phyletic Museum, Friedrich Schiller University Jena, D-07743 Jena, Germany

*Author for correspondence (emanuel.andrada@uni-jena.de)

### SUMMARY

**Previous research has resulted in increasing insight into neuro-mechanical control strategies during perturbed locomotion. In contrast, more general analyses on simple model (template)-related parameters during avian terrestrial locomotion are still rare. Quail kinematic data obtained using X-ray videography combined with ground reaction force measurements were used as a basis to investigate how 'global' template and 'local' leg joint parameters in this small, predominantly terrestrial bird change with speed and gait. Globally, quail locomotion approximates a spring-like behavior in all investigated gaits. However, ground reaction forces are more vertically oriented, which may help to balance the trunk. At the joint level, practically all the spring-like work was found to occur in the intertarsal joint (ITJ). From walking to grounded running, the local stiffness of the ITJ decreases similarly to the reduction observed in global leg stiffness. Thus, in gaits without aerial phases the quails may modulate ITJ stiffness to regulate global leg stiffness, and therefore gait changes, to a significant degree. At higher speeds both global leg compression and stiffness are increased (the latter to values not significantly different to those obtained during walking). This enables the animals to shorten contact time and to generate aerial phases (running). However, we did not observe a change in the stiffness in the ITJ with a change of gait from grounded running to running. We hypothesize that a more extended leg at touch-down, controlled by the joint angles in the knee and ITJ, has an important influence in the leg stiffness adjustment process during running.**

Key words: avian locomotion, spring-mass, joint control, biomechanics, inverse dynamics, joint stiffness.

Received 15 January 2013; Accepted 8 July 2013

## INTRODUCTION

When birds increase speed during terrestrial locomotion, they change gait. First, birds change from walking to grounded running [a running gait without aerial phases (Rubenson et al., 2004)]. At higher speeds, most birds studied so far change from grounded running to aerial running (e.g. Cavagna et al., 1977; Gatesy and Biewener, 1991; Abourachid and Renous, 2000; Rubenson et al., 2004; Nudds et al., 2011; Stoessel and Fischer, 2012). Previous studies have shown that these transitions are often accompanied by: (1) smooth variations of spatio-temporal parameters as the speed increases (e.g. Gatesy and Biewener, 1991; Abourachid and Renous, 2000); (2) gradually increasing leg joint amplitudes with increase of speed (Gatesy and Biewener, 1991; Abourachid and Renous, 2000; Nyakatura et al., 2012; Stoessel and Fischer, 2012) and (3) a gradual shift from vaulting mechanics towards bouncing mechanics of the center of mass (CoM) (Rubenson et al., 2004; Hancock et al., 2007; Nyakatura et al., 2012). Gait changes appear to not always be correlated to changes in the metabolic energy consumption, but specialized walking/running birds utilize specific gaits at given speeds on a treadmill in correlation to energetic minima (Rubenson et al., 2004; Nudds et al., 2011). Although these studies provided important insight into speed-related changes of avian terrestrial locomotion, we still know surprisingly little about how global parameters and local parameters at the leg level vary with gait, and thus how their tuning influences gait and motor control strategies.

Global parameters describe biomechanical systems as a whole in the case of terrestrial locomotion by reducing the hindlimb to a 'virtual leg' or 'global leg' linking the hip or the CoM with the center of pressure (CoP), and by representing the complex action of muscles and tendons by a minimal number of parameters (see below). Such simple models of locomotion are often referred to as templates (Full and Koditschek, 1999). In contrast, assessing local parameters permits inference of each joint's contribution to global leg behavior. At the global level, the spring loaded inverted pendulum (SLIP) model [also called the spring-mass model (Blickhan, 1989)] can accurately describe the dynamics of running and hopping, while the bipedal spring loaded inverted pendulum (BSLIP) model (also called the bipedal spring-mass model) can predict those of moderate walking (Geyer et al., 2006; Lipfert et al., 2012) and grounded running (Andrada et al., 2012; Andrada et al., 2013), if the appropriate limb parameters for these models are given (limb angle at touch-down, leg stiffness, effective limb length and, for the BSLIP, limb compression).

One of the most investigated global leg parameters is leg stiffness. Interestingly, studies on speed-related changes in leg stiffness during human and non-human animal running leads to contradictory results. In some studies, leg stiffness has been reported to remain constant during running at different speeds both in humans and non-human animals (He et al., 1991; Farley et al., 1993). In contrast, Arampatzis and colleagues (Arampatzis et al., 1999) reported that leg stiffness increased in human running when the speed increased.

Experimental evidence shows also that when hopping or running humans encounter sudden changes in substrate stiffness or damping (Farley et al., 1998; Ferris et al., 1999; Kerdok et al., 2002; Moritz et al., 2004) or changes in terrain height (Grimmer et al., 2008; Müller and Blickhan, 2010), subjects adapt their global leg parameters to the altered situation. For example, on surfaces with lower stiffness, humans increase leg stiffness. The change in leg stiffness is indicated by a reduction in the vertical downwards motion of the CoM from touch-down (TD) to mid-stance and nearly constant maximum leg force (Farley et al., 1998; Ferris et al., 1999; Kerdok et al., 2002). Runners on uneven ground decrease leg stiffness with the increasing height of the vertical perturbation (Grimmer et al., 2008). Here, in contrast to the results obtained on compliant surfaces, change in leg stiffness is more likely to be produced by an altered leg force (Grimmer et al., 2008). In addition, the adaptation of global leg parameters during running on uneven ground seems to exploit the self-stabilizing properties of the SLIP model to stabilize locomotion (Grimmer et al., 2008; Müller and Blickhan, 2010). Valuable experiments on running birds over tracks with unexpected changes of terrain height have also been conducted (e.g. Daley et al., 2006; Daley et al., 2007). Here, the delay in ground contact resulted in a steeper but more variable angle of attack. This effect could be attributed to swing-leg retraction, which can enhance the tolerance to ground disturbances significantly (Seyfarth et al., 2003). Although leg stiffness during the unexpected drop varied dramatically (Daley et al., 2007), it remains unclear how this adjustment of leg stiffness facilitated the continuation of rhythmic striding locomotion. More general information about gait-related changes in avian leg stiffness is largely missing. In the present paper we aim to study how global leg stiffness in a small predominantly terrestrial bird changes with speed and gait, and which joints may mainly be responsible for tuning global leg stiffness.

Our first main hypothesis is that global leg stiffness may approximate a spring-mass behavior for all gaits. Contrary to humans or large animals that walk with extended legs, and thus with high leg stiffness [for humans, see Lipfert et al. (Lipfert et al., 2012)], the crouched posture observed in small animals [(e.g. Biewener, 1989; Gatesy and Biewener, 1991; Witte et al., 2002); small animals being defined as having a body mass <1 kg (following Biewener, 1989)] may enable spring-like locomotion at lower speeds. In particular, we expect that overall low stiffness is highest during walking. Joint angles undergo smaller flexions during walking as compared with running (e.g. Gatesy and Biewener, 1991; Abourachid et al., 2011; Nyakatura et al., 2012; Stoessel and Fischer, 2012). When switching from walking to grounded running, this is considered to be equivalent to a switch from stiff-legged vaulting to compliant bouncing. We also expect a transition between grounded running and running to be represented by an increase of both global leg stiffness and global leg compression, to cope with the reduced contact times and to exert higher vertical ground reaction forces (GRFs).

Our second main hypothesis is that the more distal joints [the intertarsal joint (ITJ) and the tarsometatarso-phalangeal joint (TMTJ)] are responsible for tuning global leg stiffness, and therefore play an important role in controlling gait transitions. We base this expectation on the results of previous studies that have shown in running guinea fowl that the more distal joints may act as spring-like elements, while more proximal ones (hip, knee) did not show energy storage during either level running (Daley and Biewener, 2003) or unexpected drops (Daley et al., 2007). Similarly, Rubenson and colleagues showed that ostrich store and release elastic energy mainly in the TMTJ (Rubenson et al., 2011). In humans, Kuitunen and colleagues (Kuitunen et al., 2002) observed increments in knee stiffness with increasing running speed. Others (Farley and Morgenroth, 1999; Müller et al., 2010) reported that leg stiffness during hopping and running over uneven terrain seems to depend mostly on ankle stiffness. In order to confirm our second hypothesis we expect to see a correlation between the changes observed in the global stiffness and those observed at the joint level.

We investigate this by combining kinematic data derived from X-ray motion analysis with single limb force plate measurements during locomotion of the common quail. This permits us to evaluate both the virtual leg function during stance (CoP–CoM) and joint mechanics using inverse dynamics analysis and joint kinematics.

## MATERIALS AND METHODS

### Animals

Eight adult common quails [Phasianidae: *Coturnix coturnix* (Linnaeus 1758)] weighing between 180 and 240 g were obtained from local breeders. The birds were housed in spacious cages with access to food and water *ad libitum*. The Committee for Animal Research of the State of Thuringia, Germany, approved the animal care and all experimental procedures (registry number 02-47/10).

### X-ray motion analysis

The birds moved across a 3 m long walking track at their preferred speeds. The track was covered with fine sandpaper (grit 40) to reduce slipping. We simultaneously recorded kinematics and GRFs. For the kinematic analysis, synchronized, biplanar X-ray videography (Neurostar, Siemens, Erlangen, Germany) at the facility of the Institut für Spezielle Zoologie und Evolutionsbiologie mit Phyletischem Museum, Germany, was used. X-ray recordings were taken from the latero-lateral and ventro-dorsal projections. Because of the limited size of the image intensifiers, only 38 cm of the track (including the instrumented part; see below) was visible in the X-ray recordings. Our experimental setup additionally had two synchronized standard light high-speed cameras (SpeedCam Visario g2, Weinberger, Erlangen, Germany) filming from a frontal and lateral perspective to cover a larger portion of the track. The X-ray machine operated at 40 kV and 53 mA, with a sampling frequency of 1 kHz. We filtered the raw video data (e.g. gamma correction, contrast, sharpness) and, finally, performed the digitization of the joints and other landmarks (Fig. 1A) using SimiMotion software (SimiMotion Systems, Unterschleißheim, Germany). X-ray videos suffer from distortion and were therefore corrected prior to analysis with use of a freely available MATLAB (The MathWorks, Natick, MA, USA) routine (www.xromm.org) provided by Brown University (Providence, RI, USA).

### Force data acquisition and analysis

We measured three-dimensional GRF and CoP with two custom-built (8×9 cm) force plates, which we integrated into the walking track. In order to reduce metal parts in the area of the X-ray beams, we used carbon fiber to construct the force plates and their support. We used 6-DOF (degree of freedom) force-torque sensors (ATI nano17, ATI Industrial Automation, Apex, NC, USA) as transducer elements. Using fast Fourier transformation, we measured the plates' dominant eigenfrequency, which turned out to be above 200 Hz. Furthermore, our static tests revealed the resolution of the CoP position to be below 1 mm at loads higher than 300 mN. According to the sampling rate of the kinematic data, we collected GRFs at 1 kHz (NI USB-6229 and custom software LabView 2009; National Instruments, Austin, TX, USA). We synchronized force and X-ray analysis electronically (post-trigger).

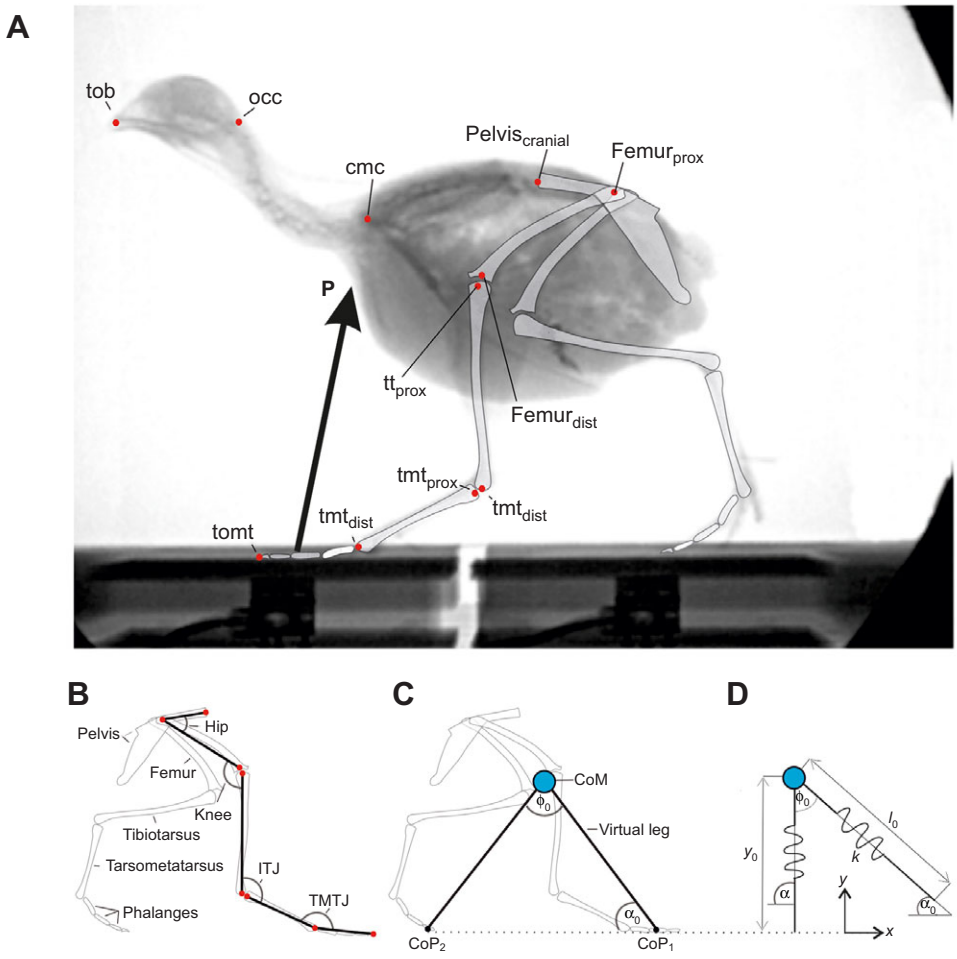


Fig. 1. Latero-lateral X-ray projection of a quail traversing the two custom-built force plates to obtain single limb kinetic data. Schematic drawing superimposed on the X-ray still image depicting all used landmarks (A) and two-dimensional representation to measure joint angles (B). **P**, instantaneous ground reaction force vector; ITJ, intertarsal joint; TMTJ, tarsometatarso-phalangeal joint; tob, tip of beak; occ, occiput; cmc, caudalmost cervical vertebrae; tomt, tip of middle toe. The TMTJ was represented by one point ($tmt_{dist}$) because of the spatial resolution of the X-ray image. (C) Virtual legs at touch-down (segments $CoP_1$–CoM–$CoP_2$). $\alpha_0$, angle of attack; $\phi_0$, aperture angle at touch-down. (D) Bipedal spring loaded inverted pendulum (BSLIP) template. $k$, stiffness; $\alpha$, leg angle with respect to the ground; $l_0$, rest length; $y_0$, initial high.

### Determination of limb element and body part properties

One of the individuals (subject 6) was euthanized and dissected. Limb elements were detached at the joints and body elements (torso, head and neck) were dissected from each other. We then weighed each element and used a pendulum method to determine each element's CoM position as described elsewhere (Nyakatura et al., 2012) (Table 2). Elements were defined using landmarks that are easy to identify in the X-ray films (Fig. 1A), and the position of the element's CoM is presented as percentage of element length measured from the proximal landmark (Table 1). The following elements and body parts were defined (from proximal to distal or cranial to caudal landmarks, respectively): thigh (femur proximal to femur distal), tibiotarsus (tibiotarsus proximal to tibiotarsus distal), tarsometatarsus (tarsometarsus proximal to TMTJ), toes (TMTJ to tip of middle toe), trunk including the wings (from caudalmost cervical vertebra to pygostyl), neck (occiput to caudalmost cervical vertebra) and head (tip of beak to occiput). For toes and tarsometatarsus the position of the CoM was assumed to be at half the length of these cylindrical elements. We also assumed a fixed CoM position between the two landmarks defining the neck, to account for the constant changes of its length due to movements of the head relative to the trunk. We used linear transformation of the data of the euthanized subject to estimate the element parameters of the other subjects in accordance with a subject's overall weight.

### Mechanics of the center of mass

To distinguish between walking and grounded running, it is necessary to assess the fluctuations of gravitational potential energy

Table 1. Limb element and body part parameters of subject 6

| Element | Mass (g) | % of total mass | Length (cm) | CoM position (% of total segment length) |
|---|---|---|---|---|
| Trunk | 173.6 | 0.724 | 7.5 | 0.5, –0.307[b] |
| Head | 7.5 | 0.031 | 4.4 | 0.328 |
| Neck | 17.7 | 0.074 | Variable[c] | 0.32 |
| Femur (thigh) | 11.1 | 0.046 | 4.1 | 0.483 |
| Tibiotarsus | 7.1 | 0.029 | 5.18 | 0.35 |
| Tarsometatarsus | 1.6 | 0.007 | 3.5 | 0.5[a] |
| Toes | 0.6 | 0.003 | 3.9 | 0.5[a] |

Relative position (from proximal) of the element's center of mass (CoM) is given as percentage of overall length.
[a]Value assumed.
[b]The CoM position of the trunk is more ventral than the line between the pygostyl and caudalmost cervical vertebra.
[c]Because of movements of the head relative to the trunk, the length of the neck changes during locomotion.

($E_p$) and kinetic energy ($E_k$) of the body's CoM due to the gradual shift of kinematic parameters between both gaits (Gatesy and Biewener, 1991; Stoessel and Fischer, 2012). Moreover, it has been demonstrated that terrestrial locomotion in small birds rarely approaches the ideal cases of either in-phase or out-of-phase fluctuation of both energy forms (e.g. Hancock et al., 2007; Nyakatura et al., 2012) as proposed to define walking and running mechanics (e.g. Cavagna et al., 1977; Heglund et al., 1982; Blickhan and Full, 1992). For the purposes of this study we categorized all trials as walking, grounded running or running. We relied on the percentage of congruity (%Congruity), as proposed by Ahn et al. (Ahn et al., 2004), between $E_p$ and $E_k$ to discriminate running from walking. This parameter more closely compares the form of the graphs for $E_p$ and $E_k$ and therefore was suggested to reflect the phase relationship better than a mere comparison of the local minima as in the calculation of phase shift. %Congruity is calculated using the product of instantaneous changes (here video frames) between $E_p$ and $E_k$. All cases of a product greater than zero, that is, when the two energies are congruent, are summed and reported as the percentage of overall frames. Ideally, %Congruity would be 100% in a running trial and 0% in a walking trial. We defined walking for %Congruity values <50 and running for %Congruity values >50. For values close to 50% we further analyzed the shape and value of the GRF, and vertical speed change of CoM at mid-stance (anterior-posterior GRF, $F_x$=0). In running, i.e. bouncing mechanics, the CoM's vertical speed changes from negative to positive at mid-stance. For symmetric steady-state walking, the vertical GRF has to be lower than body weight (1 BW) at mid-stance (M-shape), and the CoM's vertical speed changes from positive to negative at mid-stance, i.e. vaulting mechanics. We are aware of the fact that asymmetries, as usually observed in animal locomotion, will slightly shift the local extremes of the force patterns and thus the transition speed.

We calculated the instantaneous position of the body's CoM from kinematic data (X-ray motion analysis data of the limbs, additional kinematic data of digitized head, neck and torso landmarks, and each element's CoM position). To validate the kinematic analysis, we also determined the CoM trajectory by double integration of the anterior-posterior and vertical accelerations ($a_x$, $a_y$) obtained from the measured GRF divided by body mass. As initial positions of the CoM ($s_{0x}$, $s_{0y}$), we used those obtained kinematically. Because kinematic methods do not account for movement of appendages and viscera, kinematically determined CoM initial speeds ($v_{0x}$, $v_{0y}$) are imprecise for use as integration constants. Thus, we optimized CoM initial speed estimates by minimizing the sum of squared distances between the kinematically determined CoM trajectory and the CoM trajectory derived from force plate analysis as described in previously (Daley et al., 2007). For locomotion close to steady state, both methods match (Fig. 2A).

### Global and local leg stiffness

The global analysis is based on the BSLIP template (Geyer et al., 2006). The BSLIP model consists of the body as a point mass $m$ at the CoM and two massless, linear springs with a given stiffness $k$ and rest length $l_0$ describing the action of the legs during stance. Each spring acts independently, and the swing phase is used to adjust the angle of attack $\alpha_0$ related to the ground or the aperture angle $\phi_0$ related to the stance leg (Fig. 1D). Motion is restricted to the sagittal plane, hence the equations of motion of the CoM are:

$$m\ddot{\mathbf{x}} = -k(l_0 - l_1)\cos\alpha_1 - k(l_0 - l_2)\cos\alpha_2 , \quad (1)$$

$$m\ddot{\mathbf{y}} = -m\boldsymbol{g} + k(l_0 - l_1)\sin\alpha_1 + k(l_0 - l_2)\sin\alpha_2 , \quad (2)$$

where $\ddot{\mathbf{x}}$ and $\ddot{\mathbf{y}}$ are the accelerations of the CoM, $m$ is the body mass, $\boldsymbol{g}$ is the gravitational acceleration, $l_1$ and $l_2$ are the instantaneous leg lengths during stance, and $\alpha_1$ and $\alpha_2$ are the corresponding orientations between the ground and each leg. In the single-support phase, only one leg exerts force and the right-hand-most term in both equations is zero, whereas in the double-support phase, both legs exert force and hence all right-hand terms in both equations are nonzero. During aerial phases, the trajectory of the center of mass is influenced only by the gravitational force.

To estimate the global leg stiffness $k$ from experimental data, we computed first the instantaneous virtual leg length as the distance between CoM and CoP. As virtual leg length is normally non-symmetrical relative to TD and take-off (TO) events, we averaged relative virtual leg lengths in order to determine the global leg stiffness $k$ from kinetic data. We computed $k$ as $k$=$\mathrm{GRF}_{\text{mid-stance}}/\Delta l$, where $\Delta l$=$(l_{\text{leg,TD}}+l_{\text{leg,TO}})/2-l_{\text{leg,mid-stance}}$. Note that $l_0$=$(l_{\text{leg,TD}}+l_{\text{leg,TO}})/2$ is the rest length of the assumed spring (Fig. 3). This approach assumes that the virtual leg behaves like a linear spring. To enable comparison with other species, we present global and local parameters in dimensionless form, following Andrada and co-workers (Andrada et al., 2012; Andrada et al., 2013). Dimensionless global leg stiffness was defined as $\hat{k}=kl_0/m\boldsymbol{g}$. The dimensionless global leg compression ($\psi$) related to the compression of the spring at mid-stance is equal to

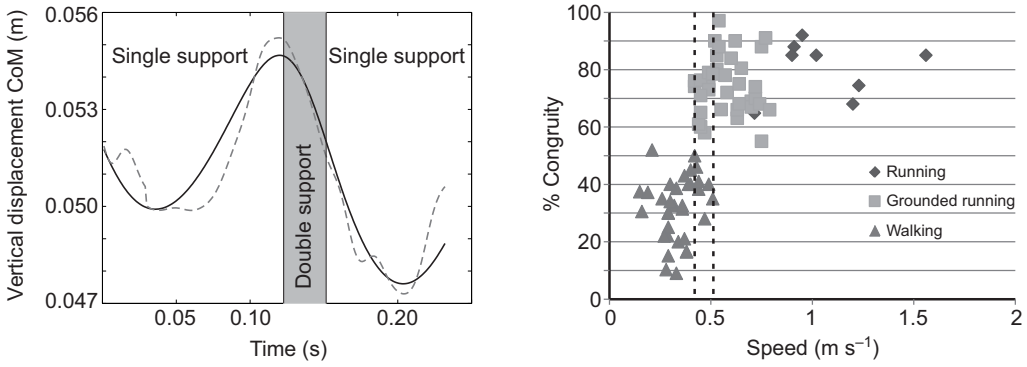


Fig. 2. (A) Estimation of vertical displacement of the CoM for a grounded running trial of a quail (gray dashed line, combining kinematics and cadaveric information; black solid line, using integration of GRF). (B) %Congruity *versus* speed. %Congruity was used to distinguish between walking and running gaits. We defined walking as %Congruity values <50 and running as %Congruity values >50. Trials with %Congruity close to 50 were further analyzed to differentiate walking and running (shape of GRF, vertical speed change close to mid-stance; see Materials and methods). Vertical dashed lines depict overlapping speeds where walking and grounded running occur.

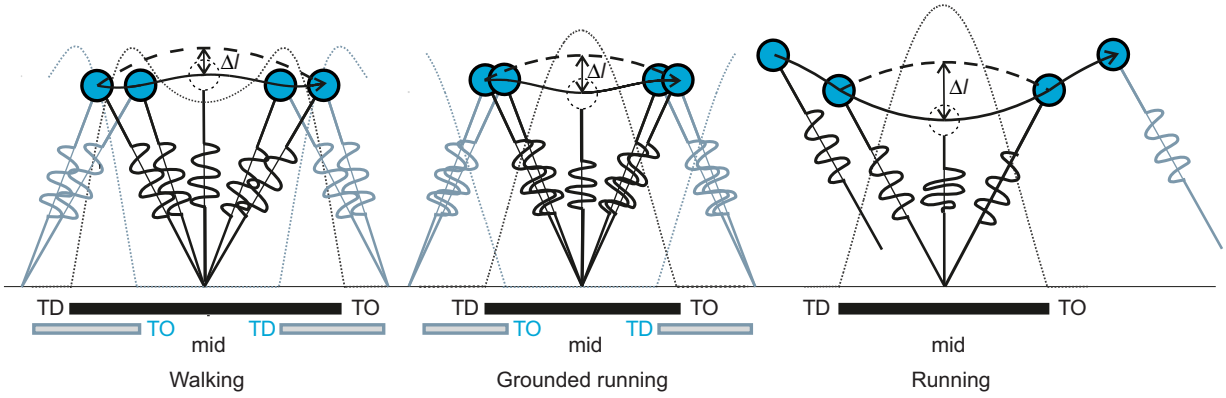


Fig. 3. Estimating single-leg stiffness $k$ during walking, grounded running and running, based on the BSLIP template (black, leg 1; gray, leg 2). At touch-down (TD) and take-off (TO) events, the 'virtual leg' linking the CoM with the CoP is equivalent to the rest length of a spring $l_0$; during stance, the virtual leg length is compressed to exert the leg's GRF. The dashed arcs show the trajectory of $l_0$, the solid curves the trajectory of the CoM, and the dotted curves the vertical component of the GRF. For all three gaits, the stiffness $k$ can be estimated, assuming linear behavior, as $k$=GRF/Δ$l$. By choosing mid-stance (mid), only the vertical component of the GRF and Δ$l$ are needed to estimate $k$. Note that although stiffness is measured for single legs, the model is bipedal for walking as well as for grounded running.

the GRF in body weight [$\psi$=GRF/$mg$=$k(l_0-l)/mg$ (see Andrada et al., 2012; Andrada et al., 2013)].

We determined the angle of attack at touch-down ($\alpha_0$) between the ground and the segment CoM–CoP as shown in Fig. 1C, and the aperture angle $\phi_0$ at touch-down, following Andrada and colleagues (Andrada et al., 2013), by computing the angle between the CoPs of the stance legs and the CoM (Fig. 1C). We measured limb segmental angles related to the ground, and joint angles as shown in Fig. 1B.

Global leg properties must be generated locally at the joint level. Calculation of local stiffness requires estimates of joint torques. We estimated torque at each joint during stance using a quasi-static analysis neglecting segment inertia and weight. Especially during slow locomotion, the error in estimating joint torques from GRF should be negligible (as linear and rotational accelerations are low). Moreover, Witte and co-workers showed that for small mammals even during fast locomotion the inertia of the extremities only contribute a maximum of 10% to overall forces (Witte et al., 2002). In our case, even at the maximal running speed measured, the influence of the femur segment's moment of inertia to the joint torque, estimated as a thin rod $J_f\ddot{\theta}_f=[(m_f l_f^2)/3]\ddot{\theta}_f$, is lower than 5% of the maximal observed torque (cf. Fig. 7). Here, $J_f$ represents the moment of inertia, $l_f$ the length and $m_f$ the mass of the femur (see Table 1); $\ddot{\theta}$ represents the maximal angular acceleration of the segment measured during running (800 s$^{-2}$). Thus, external torque was computed as the magnitude of the cross-product between the instantaneous joint position vector relative to the position of the CoP, and the instantaneous GRF vector P (knee and ITJ instantaneous joint positions were assumed to be located in the middle between the distal and proximal ends of adjacent bones; while hip and TMTJ joints were assumed to be located at the proximal tip of the femur and the distal tip of the tarso-metatarsus, respectively).

### Data analysis

For final data analysis we were able to obtain a total of 74 steady-state strides (32 walking, 34 grounded running and eight running) of biplanar X-ray recording and synchronous, single limb SRF traces. For our investigation of steady-state locomotion we discarded all trials with a horizontal speed deviation of more than 5% during stance. Trials fulfilling this criterion were the exception. Approximately 10 trials were necessary to obtain a single steady-state trial with both feet not overstepping one of the plates. In most cases these successful trials were grounded runs or walking trials, while aerial running was rarely used by the quails [note that in previously published treadmill studies, quails never ran using aerial phases (cf. Gatesy and Biewener, 1991; Stoessel and Fischer, 2012)]. We used $t$-tests to determine whether maximal joint torques, linear and rotational stiffness are gait related (significance level $P$<0.05) in SPSS 18 (IBM, Armonk, NY, USA).

### Simulations

Subsequently, we performed BSLIP forward simulations using the mean values of the global parameters obtained experimentally to test for differences between observed data and the linearity assumptions of the BSLIP. We compared GRFs, leg length variation and contact time from both experimental and BSLIP results during walking, grounded running and aerial running. For walking and grounded running, simulations started at mid-stance ($x_0$=0 and $v_{0y}$=0). Running simulation started at the apex ($y_{max}$, $x_0$=0, $v_{0y}$=0). $v_{0x}$, $k$, $l_0$ and $\phi_0$ or $\alpha_0$ were set according to the experimental data, while the initial high $y_0$ was set to match as best as possible the value of the GRF/$mg$=$\psi$ at mid-stance. For walking and running, we applied the commonly used angle of attack as the TD strategy. For grounded running, the aperture angle between legs was preferred (following Andrada et al., 2012; Andrada et al., 2013).

Applying the fixed aperture angle $\phi_0$ between legs, the TD of the swing leg occurs when $y=l_0\sin(\alpha-\phi_0)$, where $\alpha$ is the instantaneous stance leg angle with respect to the ground measured clockwise (Fig. 1D). In contrast, using the fixed angle of attack $\alpha_0$, TD of the swing leg occurs when $y=l_0\sin\alpha_0$. TO occurs when the spring force becomes zero. During running we ensure that only one leg can land at a time. We implemented the simulation model in MATLAB/SIMULINK (The MathWorks). To integrate Eqns 1 and 2 we applied a Runge–Kutta variable-step algorithm (ode45) with a relative and absolute integrator error tolerance of 1e–9.

## RESULTS

Walking was observed at speeds ranging from 0.15 to 0.51 m s$^{-1}$ with a mean of 0.34 m s$^{-1}$, grounded running at speeds between 0.42 and 0.79 m s$^{-1}$ with a mean of 0.58 m s$^{-1}$, and aerial-phase running gaits at speeds ranging from 0.75 to 1.56 m s$^{-1}$ with a mean of 1.06 m s$^{-1}$. The walking–grounded running transition showed a speed

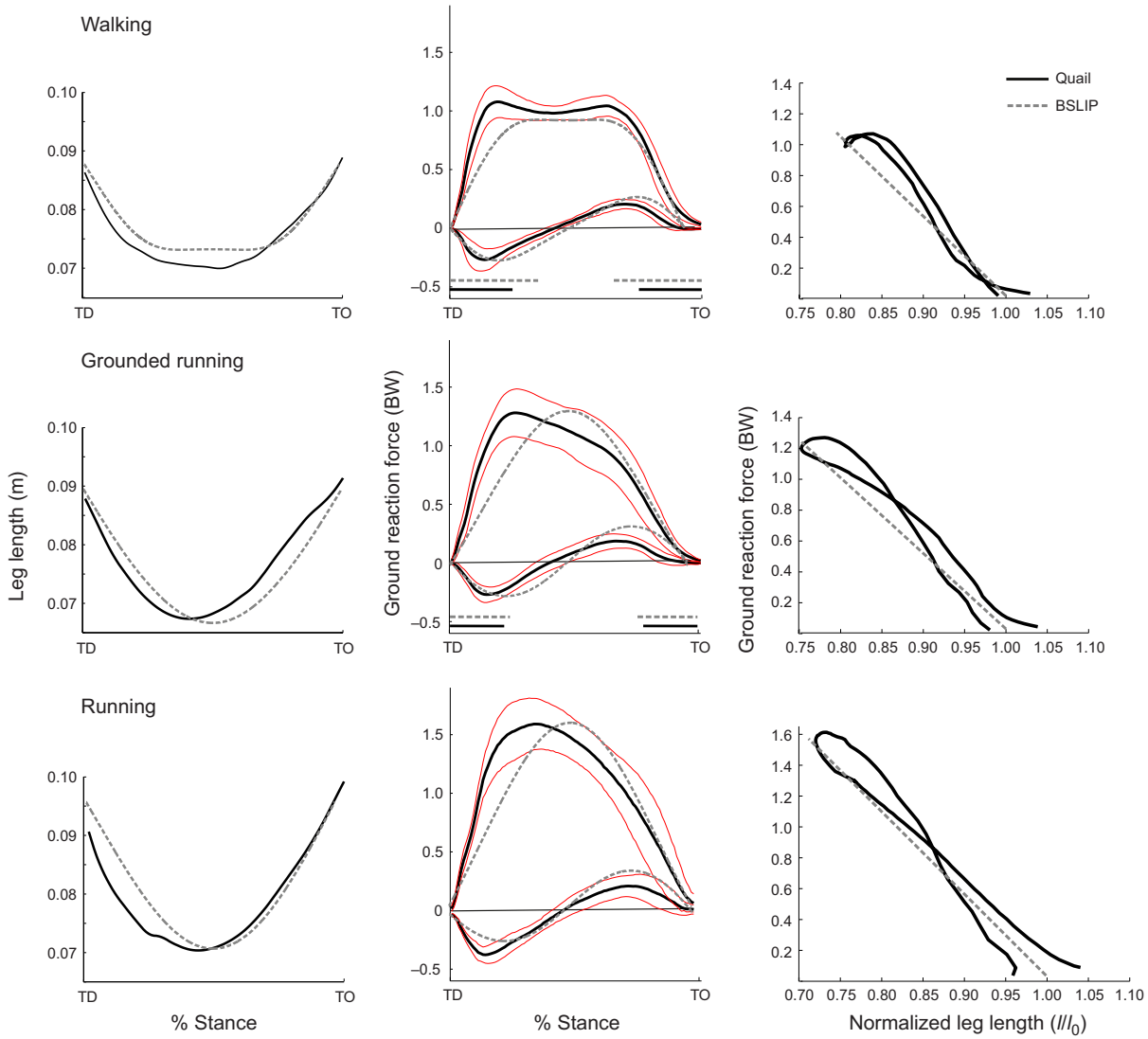


Fig. 4. Global leg parameters during terrestrial locomotion of the quail *versus* BSLIP simulation predictions. Solid lines represent experimental findings; gray dashed lines represent the BSLIP model. Leg length variation (left), vertical and anterior-posterior GRFs (middle) and force–length plots (right) during walking (top), grounded running (middle) and running (bottom). The GRF and force–length plots are presented as means (walking, $N$=32; grounded running, $N$=34; running, $N$=8). GRF plots also include ±1 s.d., and horizontal lines represent relative double support phases (walking and grounded running). For the force–length plots, resultant force is used. $l_0$ in the force–length plots refers to the mean value of $l_0$ for each gait (see Table 2). Simulation parameters: walking, $v_{x0}$=0.34 m s$^{-1}$, $\hat{k}$=5.8, $l_0$=0.087 m, $E$=0.168 J, $\alpha_0$=58 deg; grounded running: $v_{0x}$=0.59 m s$^{-1}$, $\hat{k}$=5, $l_0$=0.089 m, $E$=0.191 J, $\phi_0$=65 deg; running: $v_{0x}$=1.06 m s$^{-1}$, $\hat{k}$=6.2, $l_0$=0.096 m, $E$=0.286 J, $\alpha_0$=57 deg. Caution is needed when interpreting results of simulations for walking: a less compressed spring-leg at mid-stance would pronounce the vertical GRF's M-shape and simultaneously diminish the relative duration of double support phases.

overlap of 0.09 m s$^{-1}$. The grounded running–running transition seems to be more defined (just one running trial overlapped with grounded running speeds; Fig. 2B).

The vertical component of the GRF we obtained for the quails displayed the well-known M-shape for walking, a positive skewed half-sine pattern for grounded running, and a less skewed half-sine shape for running (Fig. 4). Notably, at very slow walking speeds the vertical component of the GRF displayed a three-peaked shape, as predicted by the BSLIP model (Geyer et al., 2006) but uncommon in human bipedalism (Fig. 5). Anterior-posterior GRFs approximated negative sine waves for the different gaits.

### Gait-related changes in global parameters

The asymmetry of the virtual leg length between TD and TO events increased with speed (Fig. 4). While the angle of attack was not significantly different between gaits, the aperture angle varied significantly between walking and grounded running (Table 2). The value $l_0$, associated with the rest length of the spring in the (B)SLIP model, was similar for walking and grounded running, but significantly longer for running (Table 2). Leg stiffness decreased significantly from walking to grounded running and increased again significantly at running gaits. Interestingly, leg stiffness during walking and running did not differ significantly, while global leg compression increased with speed and was significantly different between gaits (Table 2). Our findings show two important deviations between experimental data and (B)SLIP model assumptions. The first is that GRFs are not directed to the CoM as expected for the (B)SLIP model, but are more vertically oriented. The second difference from the SLIP is shown by the fact that CoP is shifted cranially during stance. It starts approximately halfway between the

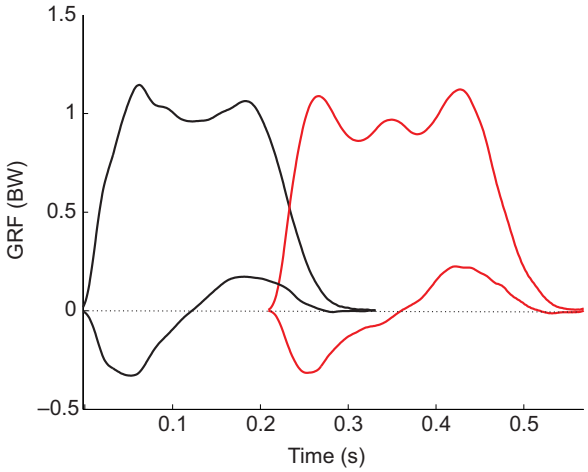


Fig. 5. Vertical and anterior-posterior GRFs obtained during slow walking. Note that vertical GRF obtained for the second stride show a three-humped profile as predicted by the BSLIP model at slow speeds. Upper lines represent vertical components of the GRF, lower lines represent anterior–posterior components of the GRF. The first stride is shown in black, while the second is shown in red.

TMTJ and the tip of the middle toe (ToMT) and moves cranially up to the ToMT during stance (Fig. 6). Nevertheless, simulation results match surprisingly well the quails' leg length variation displayed during walking, grounded running and aerial running. GRF profiles display more marked differences. These are, for grounded and aerial running, mostly related to the symmetry of the BSLIP model. In the case of walking, the M-shape of the simulated vertical GRF almost disappears, because of the spring-leg compression at mid-stance (Fig. 4). Contact times calculated in the simulation during walking and grounded running are below those obtained experimentally (walking 15% less; grounded running 25% less), while those observed and calculated for running agree (Table 2). Moreover, double support phases, expressed as percent of stance time, are overestimated in simulations (experimentally: walking 25%, grounded running 21%; simulation: walking 39%, grounded running 23%).

### Gait-related changes in local parameters

Joint angles displayed similar angle profiles in all gaits. Except for the TMTJ, all other joints were more extended at TD with increasing speed (walking, grounded-running, running; Fig. 7). The hip joint underwent a gravity-induced flexion at TD as body weight was shifted to the supporting leg. Then it was extended until the end of the stance phase. The knee joint was flexed until *ca.* 60% of stance, and then flexion was kept constant up to 90% of stance. In gaits with double support the knee was then further flexed until TO. The ITJ was flexed in the early stance phase, and then extended up to 90% of stance, where the joint was again flexed until TO in the gaits with double support. Interestingly, both knee and ITJs start with the same joint angle in each gait. The TMTJ was flexed in all gaits until *ca.* 85% of stance and afterwards extended quickly.

In Fig. 7, joint external torques during stance estimated for walking, grounded running and running are presented. In the knee joint a sinusoidal torque pattern was observed, i.e. the torque alters sign during stance and must be compensated by flexors in the first half of the stance and then by extensors. All other joints presented a half-sine torque–time relationship and must be compensated by anti-gravitational extensor moments.

While transitioning from walking to grounded running, maximal joint torques increased significantly only for the hip and ITJs. When comparing grounded running with running, maximal joint torques increased significantly for all joints with the most significant increment in the knee joint (61.6%; Table 3).

The torque–angle loops for each joint are presented in Fig. 7. The ITJ was the only joint that displayed linear-like torque–angle relationships at each gait, as expected for a rotational spring ($M=k\theta$). Following the changes observed for the global stiffness, the rotational stiffness in the ITJ decreased significantly from walking to grounded running. But between grounded running and running, it did not change (see Table 3).

## DISCUSSION

The first goal of this paper was to analyze whether variations in leg stiffness in quail, a representative small terrestrial bird, relate to the predictions of the (B)SLIP model, when the quail change gait as speed increases. The second goal was to infer the contribution of each joint to the global spring-like behavior of the legs in these small birds.

### Global parameters related to the SLIP and BSLIP model

When quails switch gait from walking to grounded running or from grounded running to running, they roughly adapt leg stiffness following the (B)SLIP model. As expected, global leg stiffness in

Table 2. Gait-related global leg parameters

| Parameter | Walking | *N* | Grounded running | *N* | Running | *N* | *P* (*t*-test) Walking *vs* grounded running | Walking *vs* running | Grounded running *vs* running |
|---|---|---|---|---|---|---|---|---|---|
| $\hat{k}$ | 5.77±1.25 | 32 | 4.99±0.67 | 34 | 6.15±0.62 | 8 | 0.004 | 0.432 | <0.001 |
| $l_0$ (m) | 0.0872±0.0087 | 32 | 0.0886±0.007 | 34 | 0.0956±0.009 | 8 | 0.793 | 0.036 | 0.022 |
| $\alpha_0$ (deg) | 58±3 | 32 | 56.7±3.6 | 34 | 57.2±3.0 | 8 | 0.277 | 0.54 | 0.74 |
| $\phi_0$ (deg) | 57.1±4.0 | 18 | 65.8±5.0 | 21 | Not defined | | <0.001 | – | – |
| $\psi$ | 0.945±0.04 | 32 | 1.2±0.112 | 34 | 1.54±0.15 | 8 | <0.001 | <0.001 | <0.001 |
| Contact time (s) | | | | | | | | | |
| Experimental quail data | 0.31±0.05 | 32 | 0.23±0.05 | 34 | 0.124±0.022 | 8 | <0.001 | <0.001 | <0.001 |
| Simulation | 0.253 | | 0.173 | | 0.121 | | | | |
| Double support time (s) | | | | | | | | | |
| Experimental quail data | 0.08±0.017 | 18 | 0.05±0.013 | 21 | – | | <0.001 | | |
| Simulation | 0.1 | | 0.041 | | | | | | |

$\hat{k}$, dimensionless global leg stiffness; $l_0$, rest length; $\alpha_0$, angle of attack; $\phi_0$, aperture angle; $\psi$, dimensionless global leg compression.
Data are means ± 1 s.d.

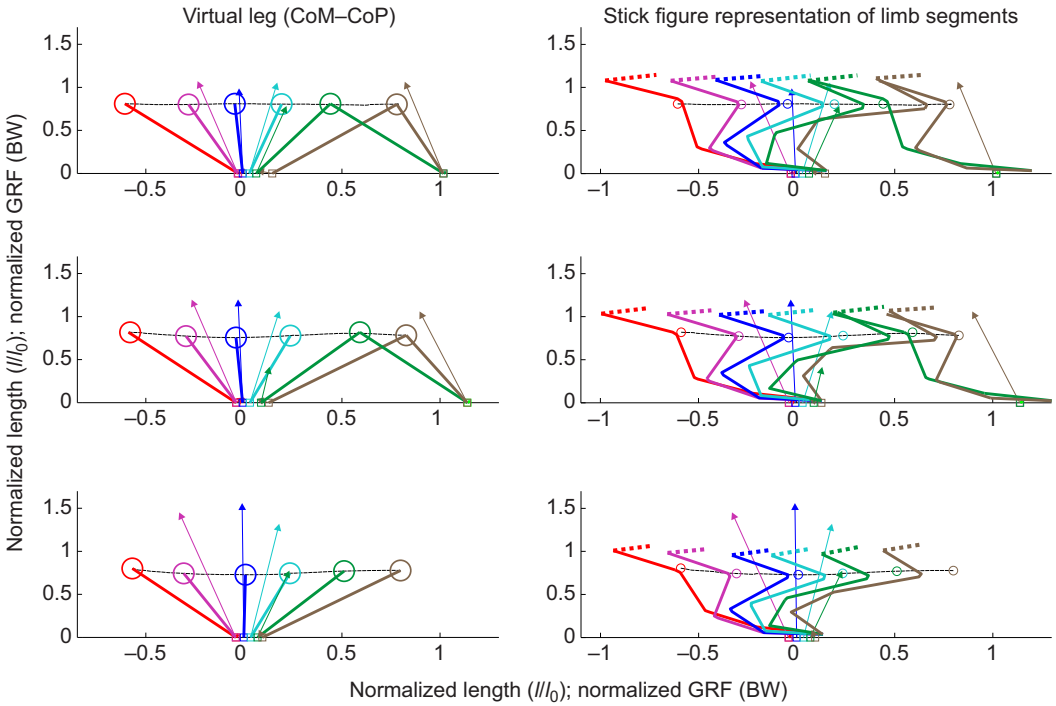


Fig. 6. Virtual and stick figure representation of limb segments together with the orientation of the GRF during walking (top, mean of 32 strides), grounded running (middle, mean of 34 strides) and running (bottom, mean of eight strides). Circles depict the position of the CoM. Segments were scaled by $l_0$ and GRF by body weight. Note that contrary to the (B)SLIP expectations, GRFs are non-collinear relative to the virtual leg and the CoP is displaced cranially during stance. Arrows represent the vector of the GRFs.

quails decreases when they change from vaulting to bouncing mechanics, and increases again during bouncing mechanics as they increase speed. Deviations from a Hookean (linear) spring are obvious especially during walking (Fig. 4, right column, top). Nevertheless, our experimental and simulation results indicate that these small birds' locomotion approximates spring-like leg behavior in all gaits. This includes slow walking speeds, at which we obtained three peaks in the shape of the vertical GRF trace, which until now were only predicted by simulations (Geyer et al., 2006). In contrast, in walking humans strong deviations occur from the spring-like leg behavior (Lipfert et al., 2012). Small birds walk and run with a more crouched posture favoring a compliant leg behavior (Gatesy and Biewener, 1991; Andrada et al., 2012; Stoessel and Fischer, 2012; present study). Although torques are relatively higher for crouched legs, the demand for high speed and/or acceleration distance per step, i.e. high locomotor performances (Günther et al., 2004), or the need to cope with rough terrain (Daley and Usherwood, 2010; Birn-Jeffery and Daley, 2012; Andrada et al., 2013), may be criteria enforcing such a leg configuration. In humans or other larger animals, swing leg inertia and decrease of effective mechanical advantage [ratio of the extensor muscle moment arm to the moment arm of the GRF (Biewener, 1989)] prevent such postures during locomotion, and grounded running is mostly avoided. Accordingly, higher stiffness and more extended legs are observed [e.g. humans $\hat{k}$>40 (Lipfert et al., 2012) *versus* $\hat{k}\cong$6 in quails at comparable Froude numbers representing walking]. The weight of the body induces an almost seven times higher compression in a quail than in a human. Interestingly, quails seem to use the same global leg stiffness during walking and running. Certainly, the more extended leg (increased $l_0$) in running is one of the factors that produced an increase of the dimensionless global leg stiffness (see 'Joint stiffness *versus* global leg stiffness', below). In a system dominated by the series compliance of passive structures, the possibilities of actuators to increase stiffness are largely reduced. This may be one of the reasons why quails, and probably other small birds, do not usually use aerial running gaits, favoring instead grounded running.

While the angle of attack remains unaltered over the three gaits, in gaits with double contact phases, the aperture angle seems to be a variable that is tuned (Andrada et al., 2013). Theoretical models show that grounded running simulated with an aperture angle strategy is less unstable and less sensitive to inaccuracies in angle tuning than the same model simulated with the angle of attack (Andrada et al., 2012; Andrada et al., 2013).

In contrast to the expectation of the spring-mass model, in which the vectors of the GRF always point to the CoM, our results show more vertically oriented forces. This vertical orientation is likely to be produced by hip torques necessary to balance the trunk. In simulations, Maus and colleagues did show that if GRFs are directed to a point located above the CoM during stance, trunk posture can be stabilized (Maus et al., 2010). In addition, a more vertical oriented GRF may result in reduced energy consumption, as elegantly presented by Usherwood and Hubel (Usherwood and Hubel, 2012). In running, torques about the CoM during stance can – with nonzero body pitch moments of inertia – reduce the mechanical work of supporting body weight by reducing horizontal forces, and thus fore–aft energy fluctuations (Usherwood and Hubel, 2012). The additional cost of balancing the trunk may be compensated for by a reduced cost to drive the energy fluctuations of the CoM.

We are aware that our method for determining stiffness (see Materials and methods and Fig. 3), especially during walking, may underestimate this parameter as non-linearities increase. Yet this method is easy to be implemented as just the vertical component of the GRF is needed. Moreover, in a different stance time leg force is overestimated as it does not point to the CoM (Fig. 6). Finally, our simulations match the quails' leg length variation and contact times reasonably well. Higher stiffness values using the linear BSLIP template would certainly diminish matching of those parameters.

### Joint torques

Net limb joint torques in humans and quadrupedal mammals generally reflect the need to counteract gravity (Winter, 1995; Witte et al., 2002; Nyakatura and Andrada, 2013). Necessary extensor

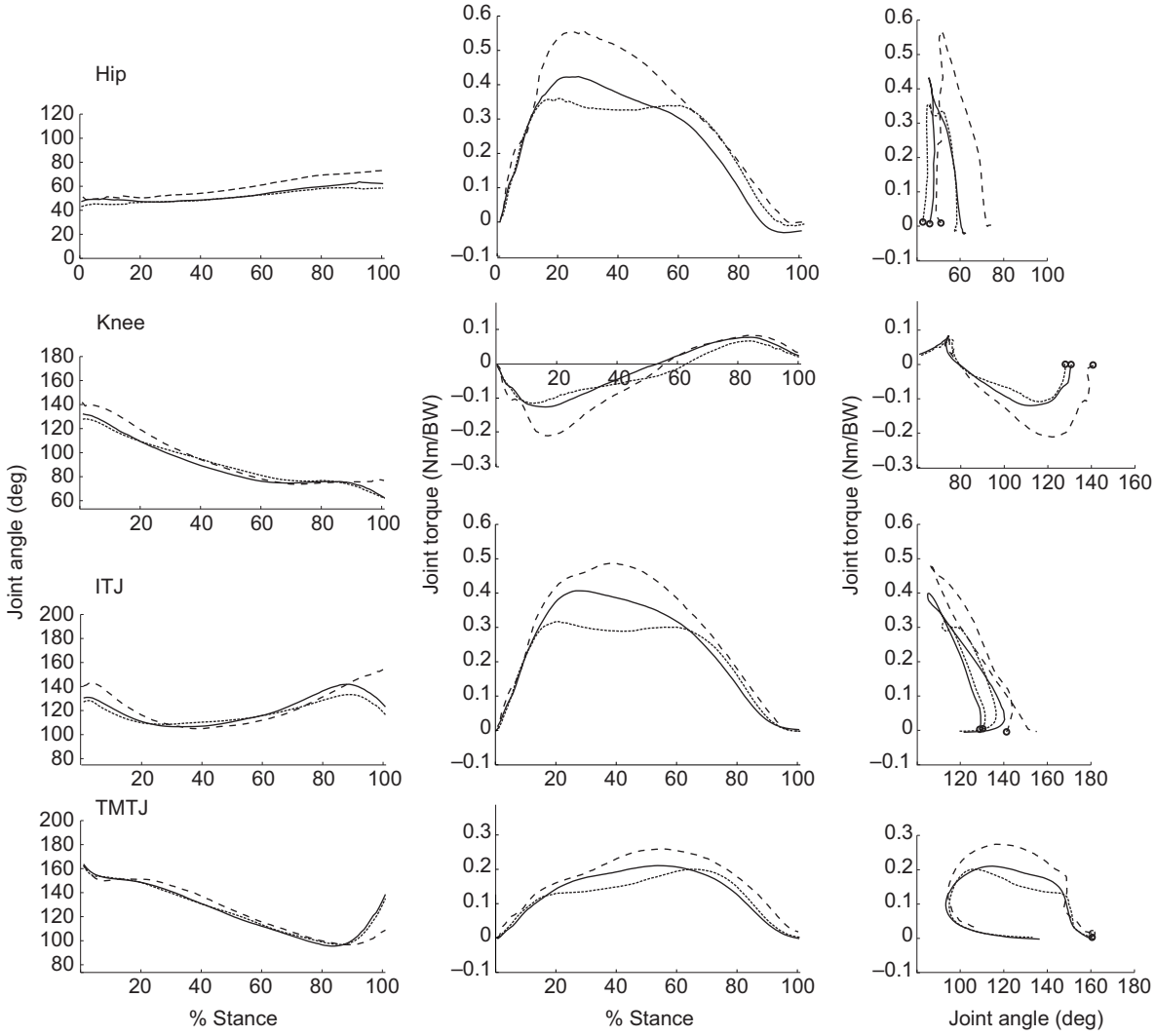


Fig. 7. Local leg parameters (joint mechanics) during terrestrial locomotion of the quail (walking, dotted line; grounded running, solid line; running, dashed line). Joint angles (left), joint torques (middle) and torque–angle plots (right) over the course of the stance for the hip, knee, ITJ and TMTJ. Displayed are mean values (walking, 32 strides; grounded running, 34 strides; running, eight strides). Increasing joint angles indicate extension, and positive values in the torque plots represent extensor torques. Circles indicate touch-down.

torques result from the 'anti-gravity role' of limb joint extensors to prevent gravity-induced limb collapse during weight bearing (Cohen and Gans, 1975; Jenkins and Weijs, 1979; Goslow et al., 1981). With the exception of the knee, which shows a biphasic torque pattern, external torque results obtained for the hip, ITJ and TMTJ in the quail agree with these observations. Knee torques and joint angles estimated for walking, grounded running and running indicate that the knee is actively flexed from TD until after mid-stance by the knee flexors and not only by gravity (Fig. 7). The change from flexor to extensor moment occurs earlier as the speed increases. Thus, the active flexion of the knee may contribute to body propulsion. After mid-stance, the extensor torque in the knee may work against gravity, while the hip adopts the role of body propulsion as soon as the vector of the GRF is pointed behind the CoM. Interestingly, Stoessel and Fischer (Stoessel and Fischer, 2012) showed that when speed is increased, the relative kinematic contribution of the knee to the step decreases while that of the hip and ITJ increases. These results agree to some degree with the kinematic notion that striding bipedalism in extant birds at slow speeds may be characterized as knee-driven (e.g. Gatesy, 1999; Hutchinson and Allen, 2009). The knee-driven mechanism is often linked to a more cranially positioned CoM and a more horizontal oriented femur (Gatesy, 1999; Hutchinson and Allen, 2009) in birds in comparison with humans.

The increased knee flexion observed may be explained by the action of the biarticular M. gastrocnemius (MG) in combination with the bird specific leg geometry. In birds, the lateral gastrocnemius muscle (LG) solely flexes the knee (Higham et al., 2008). The crouched posture increases the moment arm of this muscle. Consequently, the knee joint is more susceptible to flexion from flexor muscle activity. To antagonize this effect in the late stance, the modulation of the joint stiffness has to be achieved by knee extensor muscles, for example, the medial part of the MG [see below and Higham et al. (Higham et al., 2008)], M. femoro-tibialis or M. ilio-tibialis. Flexor knee torques in the early stance phase were also observed in running guinea fowl (Daley et al., 2007) and ostriches (Rubenson et al., 2011). Ostriches have more extended legs, and the knee is only flexed until *ca.* 20% of the stance followed by a strong extension (see Rubenson et al., 2007; Rubenson et al., 2011). In human locomotion, depending on the knee joint angle, the MG

Table 3. Gait-related local leg parameters

| Parameter | Walking | Grounded running | Running | Walking *vs* grounded running: Increment/ decrement (%) | Walking *vs* grounded running: *P* | Walking *vs* running: Increment/ decrement (%) | Walking *vs* running: *P* | Grounded running *vs* running: Increment/ decrement (%) | Grounded running *vs* running: *P* |
|---|---|---|---|---|---|---|---|---|---|
| Torque TMTJ | 0.207±0.05 | 0.221±0.036 | 0.261±0.041 | 6.8 | 0.23 | 26.1 | 9.008 | 18.1 | 0.009 |
| Torque ITJ | 0.343±0.086 | 0.407±0.054 | 0.503±0.063 | 18.7 | 0.001 | 46.7 | <0.001 | 23.6 | <0.001 |
| Torque knee | 0.129±0.051 | 0.138±0.037 | 0.223±0.06 | 7 | 0.44 | 72.9 | <0.001 | 61.6 | <0.001 |
| Torque hip | 0.399±0.078 | 0.451±0.061 | 0.581±0.06 | 13 | 0.004 | 45.6 | <0.001 | 28.8 | <0.001 |
| Rotational stiffness ITJ | 0.014±0.004 | 0.011±0.002 | 0.011±0.003 | –20 | 0.01 | –20.7 | 0.096 | –0.9 | 0.92 |

Values presented are means ± 1 s.d. of maximal torques for each joint and the rotational stiffness for the intertarsal joint (ITJ) at each gait. Torques are displayed in Nm kg$^{-1}$, and the rotational stiffness in Nm kg$^{-1}$ deg$^{-1}$. *P*-values are from *t*-tests.

may act as a knee flexor or as a knee extensor (Ertelt et al., 2011). At knee joint angles between 150 and 180 deg, Ertelt et al. observed that the MG works as a knee extensor, but below 150 deg the contraction of this muscle will work against knee extension (Ertelt et al., 2011). Thus, the extended leg in humans prevents the knee flexing action of the MG and it may even extend the knee. In contrast, the medial head of the avian gastrocnemius generally wraps right around the knee and is a knee extensor even at flexed knee angles (Higham et al., 2008). However, the insertions of the LG and MG act about the ankle joint *via* a common tendon. Thus, the contraction of both parts of the MG extends the ITJ joint, for which – together with the hip joint – we found the biggest extensor torques.

Our findings show that, on average, bouncing leg behavior demands significantly higher torques in the hip (13.0%) and ITJ (18.7%) in respect to vaulting leg behavior. However, these increments seem to be relatively moderate if we take into account that the speed increased between these two gaits on average by ~70%. Obviously, grounded running offers the advantage of long step lengths and contact times, increasing the distribution of GRFs. The result is a reduction in peak reaction forces and thus joint torques compared with gaits that feature greater limb stiffness and/or aerial phases. Energy storage and the reduction in peak force in grounded running may thus help to reduce the cost of locomotion. In contrast, the decrease in the effective mechanical advantage of the musculature may cancel out this effect (McMahon et al., 1987; Biewener, 1989). When quails run with aerial phases, maximal joint torques increase significantly. Our results show that the most important relative increment occurs, surprisingly, in the knee joint. This is likely to be produced by the significant increased force generated by the LG during running (Higham et al., 2008) that needed to cope with higher flexing moments in the ITJ.

### Joint stiffness *versus* global leg stiffness

We hypothesized the ITJ and the TMTJ to be responsible in tuning global leg stiffness. In contrast to our assumptions, the TMTJ did not display a quasi-linear torque–angle relationship, as expected for a rotational spring. This was only observed for the ITJ. The latter can largely explain the changes observed in global leg stiffness between walking and grounded running. Comparing the mean values of each gait presented in Tables 2 and 3, the rotational stiffness in the ITJ decreased by ~20% while the overall leg stiffness decreased by ~14%. In contrast, the ITJ stiffness estimated for running did not differ from values obtained for grounded running, while the leg stiffness increased by ~23% between these two gaits. This may indicate that the ITJ changes gradually between two behaviors, namely vaulting and bouncing. The observed increase may also be a cumulative result of the action of non-linearities among leg joints. The more extended leg is one of the factors that produced an increment of the dimensionless leg stiffness. First, the observed $l_0$ increase (~8%) can explain partially the increase of 20% in the dimensionless leg stiffness between these gaits. The second component may be the result of a more extended knee. Farley and colleagues discussed that the ankle stiffness is affected by the knee angle at TD, which changes the activation of the MG, M. tibialis anterior or M. soleus (Farley et al., 1998). Thus a more extended knee, as observed in our results, may result in an increase in MG force without requiring changes in the activation of that muscle (Müller et al., 2010). In addition, the more extended leg during running increases the effective mechanical advantage (Biewener et al., 2004). If activation is not altered, this results in an automatic increment in leg stiffness (Blickhan et al., 2007). Therefore, our results indicate that an important part of the leg stiffness adjustment process may rely on the leg geometry at TD, as already hypothesized (Grimmer et al., 2008; Müller and Blickhan, 2010). In this respect, morphological, electromyography as well simulation studies are needed to understand how leg geometry and joint non-linear behavior contribute to a linear-like leg stiffness.

## Conclusions

Quail terrestrial locomotion globally approximates a linear-like spring-like behavior at all investigated gaits (walking, grounded running and running), and is consistent with the predictions of the (B)SLIP model. This includes slow walking, which is characterized by a three-humped curve in the vertical GRF, as predicted by the BSLIP model (Geyer et al., 2006). Trunk balance during all gaits seems to be an important issue and thus GRFs are, in contrast to the telescopic expectation of the (B)SLIP model, more vertically oriented. As previously observed, swing leg behavior is highly conserved during all gaits (e.g. Gatesy and Biewener, 1991; Nyakatura et al., 2012; Stoessel and Fischer, 2012), while the retraction of the stance leg (e.g. Gatesy and Biewener, 1991; Nyakatura et al., 2012; Stoessel and Fischer, 2012), and therefore the aperture angle (Andrada et al., 2012; Andrada et al., 2013), is adapted as speed increases. At the local level, practically all the spring-like work was found to occur in the ITJ, while the active knee flexion is more likely to help in the regulation of the leg retraction. In contrast to the results from Rubenson and colleagues (Rubenson et al., 2011) from ostriches, the TMTJ in quails displayed no spring-like behavior. This may highlight a difference between large and small birds. Finally, our results show that between walking and grounded running, the stiffness in the ITJ decreases in a manner similar to that observed in global leg stiffness. Thus, in gaits without aerial phases, the ITJ stiffness significantly regulates overall leg stiffness. Accordingly, global leg compression increased

to exert higher vertical GRFs at mid-stance during grounded running compared with walking.

Higher global leg compression and thus higher leg forces permit quails to introduce aerial phases, and leg stiffness is increased (to values not significantly different to those obtained during walking) to cope with the decreasing contact times. However, the stiffness in the ITJ does not change from grounded running to running. Here, the more extended leg at TD adds to the notion that an important part of the leg stiffness adjustment process in running may rely on the leg geometry at TD, controlled by the joint angles in the knee and ITJ.

## ACKNOWLEDGEMENTS

We thank Roy Müller for stimulating and helpful discussions that led to the first manuscript of this work. We thank our colleagues Vivian Allen, Brandon Kilbourne and Alexander Stoessel for providing helpful critiques on early drafts of the manuscript. Rommy Petersohn and Ingrid Weiß helped with X-ray data acquisition. Three reviewers' comments helped to improve and clarify the manuscript. Fig. 3 is based on a sketch provided by reviewer 3 and the Editor (A. A. Biewener).

## AUTHOR CONTRIBUTIONS

E.A. and R.B. conceived the study; E.A. and J.A.N. designed and conducted the experiments; E.A., J.A.N. and F.B. analysed the data; and E.A. conducted simulations and drafted the manuscript. All authors contributed to the interpretation of the results and revised the manuscript.

## COMPETING INTERESTS

No competing interests declared.

## FUNDING

This research was supported by DFG (German Research Council) grants Bl 236/22-1 (E.A., F.B., R.B.) and Fi 410/15-1 (J.A.N.).

## REFERENCES

**Abourachid, A. and Renous, S.** (2000). Bipedal locomotion in ratites (Paleognatiform): examples of cursorial birds. *Ibis* **142**, 538-549.
**Abourachid, A., Hackert, R., Herbin, M., Libourel, P. A., Lambert, F., Gioanni, H., Provini, P., Blazevic, P. and Hugel, V.** (2011). Bird terrestrial locomotion as revealed by 3D kinematics. *Zoology* **114**, 360-368.
**Ahn, A. N., Furrow, E. and Biewener, A. A.** (2004). Walking and running in the red-legged running frog, *Kassina maculata*. *J. Exp. Biol.* **207**, 399-410.
**Andrada, E., Nyakatura, J. A., Müller, R., Rode, C. and Blickhan, R.** (2012). Grounded running: an overlooked strategy for robots. In *Autonomous Mobile Systems 2012*, pp. 79-87: Berlin: Springer-Verlag.
**Andrada, E., Rode, C. and Blickhan, R.** (2013). Grounded running in quails: Simulations indicate benefits of observed fixed aperture angle between legs before touch-down. *J. Theor. Biol.* **335C**, 97-107.
**Arampatzis, A., Brüggemann, G. P. and Metzler, V.** (1999). The effect of speed on leg stiffness and joint kinetics in human running. *J. Biomech.* **32**, 1349-1353.
**Biewener, A. A.** (1989). Scaling body support in mammals: limb posture and muscle mechanics. *Science* **245**, 45-48.
**Biewener, A. A., Farley, C. T., Roberts, T. J. and Temaner, M.** (2004). Muscle mechanical advantage of human walking and running: implications for energy cost. *J. Appl. Physiol.* **97**, 2266-2274.
**Birn-Jeffery, A. V. and Daley, M. A.** (2012). Birds achieve high robustness in uneven terrain through active control of landing conditions. *J. Exp. Biol.* **215**, 2117-2127.
**Blickhan, R.** (1989). The spring-mass model for running and hopping. *J. Biomech.* **22**, 1217-1227.
**Blickhan, R. and Full, R. J.** (1992). Mechanical work in terrestrial locomotion. In: *Biomechanics – Structures and Systems: A Practical Approach (Practical Approach Series)* (ed. A. A. Biewener), pp. 75-96. Oxford: Oxford University Press.
**Blickhan, R., Seyfarth, A., Geyer, H., Grimmer, S., Wagner, H. and Gunther, M.** (2007). Intelligence by mechanics. *Philos. Trans. R Soc. A* **365**, 199-220.
**Cavagna, G. A., Heglund, N. C. and Taylor, C. R.** (1977). Mechanical work in terrestrial locomotion: two basic mechanisms for minimizing energy expenditure. *Am. J. Physiol.* **233**, R243-R261.
**Cohen, A. H. and Gans, C.** (1975). Muscle activity in rat locomotion: movement analysis and electromyography of the flexors and extensors of the elbow. *J. Morphol.* **146**, 177-196.
**Daley, M. A. and Biewener, A. A.** (2003). Muscle force-length dynamics during level versus incline locomotion: a comparison of in vivo performance of two guinea fowl ankle extensors. *J. Exp. Biol.* **206**, 2941-2958.
**Daley, M. A. and Usherwood, J. R.** (2010). Two explanations for the compliant running paradox: reduced work of bouncing viscera and increased stability in uneven terrain. *Biol. Lett.* **6**, 418-421.
**Daley, M. A., Usherwood, J. R., Felix, G. and Biewener, A. A.** (2006). Running over rough terrain: guinea fowl maintain dynamic stability despite a large unexpected change in substrate height. *J. Exp. Biol.* **209**, 171-187.
**Daley, M. A., Felix, G. and Biewener, A. A.** (2007). Running stability is enhanced by a proximo-distal gradient in joint neuromechanical control. *J. Exp. Biol.* **210**, 383-394.
**Ertelt, T., Ertelt, H. J. and Blickhan, R.** (2011). The geometry-critical functional dependence of M. gastrocnemius. *Int. J. Appl. Mech.* **03**, 85-98.
**Farley, C. T. and Morgenroth, D. C.** (1999). Leg stiffness primarily depends on ankle stiffness during human hopping. *J. Biomech.* **32**, 267-273.
**Farley, C. T., Glasheen, J. and McMahon, T. A.** (1993). Running springs: speed and animal size. *J. Exp. Biol.* **185**, 71-86.
**Farley, C. T., Houdijk, H. H. P., Van Strien, C. and Louie, M.** (1998). Mechanism of leg stiffness adjustment for hopping on surfaces of different stiffnesses. *J. Appl. Physiol.* **85**, 1044-1055.
**Ferris, D. P., Liang, K. and Farley, C. T.** (1999). Runners adjust leg stiffness for their first step on a new running surface. *J. Biomech.* **32**, 787-794.
**Full, R. J. and Koditschek, D. E.** (1999). Templates and anchors: neuromechanical hypotheses of legged locomotion on land. *J. Exp. Biol.* **202**, 3325-3332.
**Gatesy, S. M.** (1999). Guineafowl hind limb function. I: Cineradiographic analysis and speed effects. *J. Morphol.* **240**, 115-125.
**Gatesy, S. M. and Biewener, A. A.** (1991). Bipedal locomotion: effects of speed, size and limb posture in birds and humans. *J. Zool. (Lond.)* **224**, 127-147.
**Geyer, H., Seyfarth, A. and Blickhan, R.** (2006). Compliant leg behaviour explains basic dynamics of walking and running. *Proc. Biol. Sci.* **273**, 2861-2867.
**Goslow, G. E., Jr, Seeherman, H. J., Taylor, C. R., McCutchin, M. N. and Heglund, N. C.** (1981). Electrical activity and relative length changes of dog limb muscles as a function of speed and gait. *J. Exp. Biol.* **94**, 15-42.
**Grimmer, S., Ernst, M., Günther, M. and Blickhan, R.** (2008). Running on uneven ground: leg adjustment to vertical steps and self-stability. *J. Exp. Biol.* **211**, 2989-3000.
**Günther, M., Keppler, V., Seyfarth, A. and Blickhan, R.** (2004). Human leg design: optimal axial alignment under constraints. *J. Math. Biol.* **48**, 623-646.
**Hancock, J. A., Stevens, N. A. and Biknevicius, A. R.** (2007). Whole-body mechanics and kinematics of terrestrial locomotion in the elegant-crested tinamou, *Eudromia elegans*. *Ibis* **149**, 605-614.
**He, J. P., Kram, R. and McMahon, T. A.** (1991). Mechanics of running under simulated low gravity. *J. Appl. Physiol.* **71**, 863-870.
**Heglund, N. C., Cavagna, G. A. and Taylor, C. R.** (1982). Energetics and mechanics of terrestrial locomotion. III. Energy changes of the centre of mass as a function of speed and body size in birds and mammals. *J. Exp. Biol.* **97**, 41-56.
**Higham, T. E., Biewener, A. A. and Wakeling, J. M.** (2008). Functional diversification within and between muscle synergists during locomotion. *Biol. Lett.* **4**, 41-44.
**Hutchinson, J. R. and Allen, V.** (2009). The evolutionary continuum of limb function from early theropods to birds. *Naturwissenschaften* **96**, 423-448.
**Jenkins, P. A. and Weijs, W. A.** (1979). The functional anatomy of the shoulder in the Virginia opossum (*Didelphis virginiana*). *J. Zool.* **188**, 379-410.
**Kerdok, A. E., Biewener, A. A., McMahon, T. A., Weyand, P. G. and Herr, H. M.** (2002). Energetics and mechanics of human running on surfaces of different stiffnesses. *J. Appl. Physiol.* **92**, 469-478.
**Kuitunen, S., Komi, P. V. and Kyröläinen, H.** (2002). Knee and ankle joint stiffness in sprint running. *Med. Sci. Sports Exerc.* **34**, 166-173.
**Lipfert, S. W., Günther, M., Renjewski, D., Grimmer, S. and Seyfarth, A.** (2012). A model-experiment comparison of system dynamics for human walking and running. *J. Theor. Biol.* **292**, 11-17.
**Maus, H. M., Lipfert, S. W., Gross, M., Rummel, J. and Seyfarth, A.** (2010). Upright human gait did not provide a major mechanical challenge for our ancestors. *Nat. Commun.* **1**, 70.
**McMahon, T. A., Valiant, G. and Frederick, E. C.** (1987). Groucho running. *J. Appl. Physiol.* **62**, 2326-2337.
**Moritz, C. T., Greene, S. M. and Farley, C. T.** (2004). Neuromuscular changes for hopping on a range of damped surfaces. *J. Appl. Physiol.* **96**, 1996-2004.
**Müller, R. and Blickhan, R.** (2010). Running on uneven ground: leg adjustments to altered ground level. *Hum. Mov. Sci.* **29**, 578-589.
**Müller, R., Grimmer, S. and Blickhan, R.** (2010). Running on uneven ground: leg adjustments by muscle pre-activation control. *Hum. Mov. Sci.* **29**, 299-310.
**Nudds, R. L., Folkow, L. P., Lees, J. J., Tickle, P. G., Stokkan, K. A. and Codd, J. R.** (2011). Evidence for energy savings from aerial running in the Svalbard rock ptarmigan (*Lagopus muta hyperborea*). *Proc. Biol. Sci.* **278**, 2654-2661.
**Nyakatura, J. A. and Andrada, E.** (2013). A mechanical link model of two-toed sloths: no pendular mechanics during suspensory locomotion. *Acta Theriol.* **58**, 83-93.
**Nyakatura, J. A., Andrada, E., Grimm, N., Weise, H. and Fischer, M. S.** (2012). Kinematics and center of mass mechanics during terrestrial locomotion in northern lapwings (*Vanellus vanellus*, Charadriiformes). *J. Exp. Zool. A* **317**, 580-594.
**Rubenson, J., Heliams, D. B., Lloyd, D. G. and Fournier, P. A.** (2004). Gait selection in the ostrich: mechanical and metabolic characteristics of walking and running with and without an aerial phase. *Proc. Biol. Sci.* **271**, 1091-1099.
**Rubenson, J., Lloyd, D. G., Besier, T. F., Heliams, D. B. and Fournier, P. A.** (2007). Running in ostriches (*Struthio camelus*): three-dimensional joint axes alignment and joint kinematics. *J. Exp. Biol.* **210**, 2548-2562.
**Rubenson, J., Lloyd, D. G., Heliams, D. B., Besier, T. F. and Fournier, P. A.** (2011). Adaptations for economical bipedal running: the effect of limb structure on three-dimensional joint mechanics. *J. R. Soc. Interface* **8**, 740-755.
**Seyfarth, A., Geyer, H. and Herr, H.** (2003). Swing-leg retraction: a simple control model for stable running. *J. Exp. Biol.* **206**, 2547-2555.
**Stoessel, A. and Fischer, M. S.** (2012). Comparative intralimb coordination in avian bipedal locomotion. *J. Exp. Biol.* **215**, 4055-4069.
**Usherwood, J. R. and Hubel, T. Y.** (2012). Energetically optimal running requires torques about the centre of mass. *J. R. Soc. Interface* **9**, 2011-2015.
**Winter, D. A.** (1995). *Biomechanics and Motor Control of Human Movement*. New York, NY: John Wiley and Sons.
**Witte, H., Biltzinger, J., Hackert, R., Schilling, N., Schmidt, M., Reich, C. and Fischer, M. S.** (2002). Torque patterns of the limbs of small therian mammals during locomotion on flat ground. *J. Exp. Biol.* **205**, 1339-1353.